Adiabatic wavelength redshift by dynamic carrier depletion using *p-i-n*-diode–loaded photonic crystal waveguides

K. Kondo[1,2] and T. Baba[1]

[1]*Department of Electrical and Computer Engineering, Yokohama National University, 79-5 Tokiwadai, Hodogayaku, Yokohama 240-8501, Japan*

[2]*Photonics Integration System Research Center, Laboratory for Future Interdisciplinary Research of Science and Technology, Tokyo Institute of Technology, 4259 Nagatsuta-cho, Midoriku, Yokohama 226-8503, Japan*

(Received 22 January 2018; published 13 March 2018)

We demonstrate an adiabatic wavelength redshift using dynamic carrier depletion. Free carriers are first induced through two-photon absorption of a control pulse and then extracted by a reverse-biased *p-i-n* diode formed on a Si photonic crystal waveguide, resulting in rapid carrier depletion. A copropagating signal pulse is redshifted by the consequent increase in refractive index. We experimentally evaluated the dynamics of the carrier depletion by the pump-probe method and explored suitable conditions for adiabatic redshift. The signal's redshift was observed, and was confirmed to originate in the dynamic carrier depletion. The redshift was experimentally determined as 0.21 nm.

DOI: 10.1103/PhysRevA.97.033818

I. INTRODUCTION

Wavelength conversion can be induced by dynamic tuning of the refractive index. This phenomenon, called *adiabatic wavelength conversion*, was suggested in a theoretical demonstration of the stoplight technique [1]. Since then, adiabatic wavelength conversion itself [2–8] and its advanced functions, such as Q-factor switching [9], ultrafast delay tuning [10,11], spectrum tuning [12], pulse reflection in a moving index front and the consequent Doppler shift [13–16], pulse compression [14,17], and on-demand pulse transfer [18], have been demonstrated by many groups. Many previous experimental demonstrations have employed carrier generation through photon absorption because it is a very simple approach for changing the refractive index for an optical pulse which passes at the speed of light. All of these experiments have reported a blueshift caused by the negative index change at the instant of carrier generation. An adiabatic redshift would expand the flexibility of the tuning and capability of the above applications. However, inducing a redshift by positively changing the refractive index is a difficult task in integrated devices composed of common materials. For example, the thermal-optic effect and electrical control of the carrier-plasma effect cannot switch at sufficient speed. The optical Kerr effect can change the index at sufficient speed but induces not only the redshift at pulse rise but also the blueshift at pulse fall simultaneously. Furthermore, it is degraded by two-photon absorption (TPA) and the subsequent free-carrier absorption (FCA) in Si. In this study, a redshift induced by a positive dynamic index change is achieved by using free-carrier generation by the TPA and carrier extraction in a reverse-biased *p-n* diode embedded on a photonic crystal waveguide (PCW). The initial carriers for the following depletion are generated by a short optical control pulse. These carriers are instantly extracted by the depletion-layer field, achieving the high-speed carrier depletion of shorter than several tens of picoseconds. Furthermore, we employ a lattice-shifted PCW (LSPCW) generating low-dispersion slow-light pulses [8,19], which enhances the TPA with the square of the group index, and thereby improves the redshift. This process is carried out in a copropagating slow-light system in which we previously demonstrated an adiabatic blueshift [8]. If a redshift can be demonstrated in the same system, we can realize a bidirectional wavelength conversion in a single system.

This paper describes our approach for inducing dynamic redshift, and the device fabricated by a complementary metal-oxide semiconductor (CMOS) process. Next, we evaluate the carrier-depletion dynamics in the LSPCW by the pump-probe method. Finally, we demonstrate the adiabatic redshift in the LSPCW and investigate its dependence on the carrier dynamics.

II. PRINCIPLES AND DEVICE

Figure 1 schematizes the approach of generating the adiabatic redshift. First, the LSPCW loaded with a reverse-biased *p-n* diode receives a high-power control pulse and generates free carriers through the slow-light-enhanced TPA. The index change of the order of 0.001 is induced by a several-tens-of-watts-level control pulse. The control pulse is administered over a few picoseconds and the TPA occurs with a subpicosecond response time, meaning that the carriers are generated within the pulse duration. The generated carriers are instantly extracted by the reverse bias. The lower panel of Fig. 1 reveals a schematic of a carrier-density transition along the center line of the LSPCW. The signal pulse propagating just behind the control pulse encounters a positive index change Δn, and is consequently redshifted. In such a copropagating slow-light system, the wavelength shift $\Delta\lambda$ is given by [8]

$$\Delta\lambda = \frac{\lambda n_g \xi}{cn}\int_C \frac{\partial}{\partial t}\Delta n(z,t)dz = \frac{\lambda\xi}{n}\int_C \frac{\partial}{\partial t}\Delta n(z,t)dt, \quad (1)$$

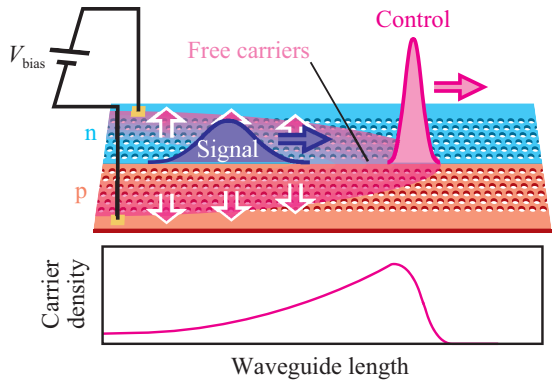

FIG. 1. Schematic of the adiabatic redshift in the LSPCW and the corresponding carrier density along the waveguide.

where n_g, c, z, and t denote the group index, the speed of light in a vacuum, position in the LSPCW, and time, respectively. $\xi \equiv (n/\omega)(\partial\omega/\partial n)$ describes the dependence of the normalized photonic band frequency on the normalized index change, where ω and n are the frequency of the light and the material index of the LSPCW, respectively. C is the trajectory of the signal pulse, which satisfies $t = (n_g/c)z$. According to Eq. (1), the redshift is enhanced by increasing the index-change rate and elongating the overlap duration of the signal pulse and dynamic carrier depletion. Hence, a large redshift requires high-speed carrier depletion and group-velocity matching between the control and signal pulses.

The LSPCW was fabricated on a silicon-on-insulator wafer by the CMOS process. The Si layer was 210 nm thick. The LSPCW was 400 μm long and cladded with SiO_2. Figure 2 is a magnified view of the center of the LSPCW and its corresponding mode profile. To obtain the low-dispersion band at an approximate wavelength of 1550 nm, we set the lattice constant a, hole diameter $2r$, and third-row lattice shift s_3 to

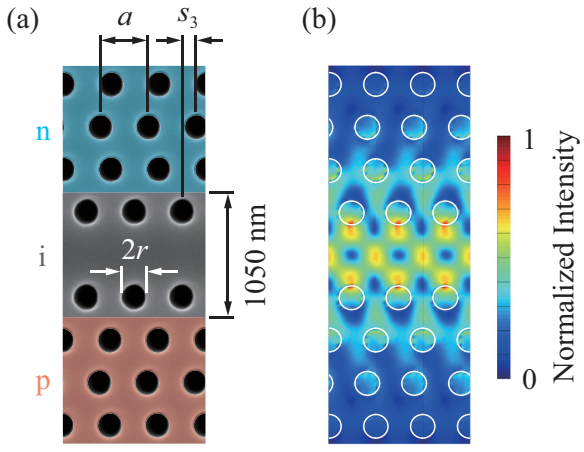

FIG. 2. Structure and characteristics of the LSPCW. (a) Shown is a top view of the fabricated LSPCW and (b) its corresponding optical intensity profile. The third-row holes (filled with SiO_2) are shifted in the propagation direction by s_3. The intensity profile was calculated by a three-dimensional finite-difference time-domain method, and was averaged over the propagation band between the photonic band gap and light cone.

400, 215, and 110 nm, respectively [20]. This device yielded $n_g \sim 24$ in the low-dispersion band. The optical pulse was sent from an external lensed fiber to the LSPCW through a spot-size converter (SSC) [19] and a Si wire waveguide with a total coupling loss of 3.5 dB. For high-speed carrier depletion, we employed a p-i-n junction, adjusting the intrinsic-region width until the depletion layer largely overlapped the optical mode corresponding to the carrier-generation profile. The p and n regions were formed by boron ion (concentration: $10.5 \times 10^{17}\,cm^{-3}$) and phosphorus ion ($6.2 \times 10^{17}\,cm^{-3}$) implantation, respectively. Furthermore, to contact the Al electrodes, deeply doped $p+$ and $n+$ regions ($1.9 \times 10^{19}\,cm^{-3}$) were formed on the outside of the p and n regions, respectively. We set the distance between the $p+$ and $n+$ regions to 3.8 μm.

III. CARRIER-DEPLETION SPEED

As described above, the large redshift is conferred by high-speed carrier depletion. We experimentally explored the conditions under which high-speed depletion occurs under the signal pulse. The carrier-depletion dynamics was evaluated by the pump-probe method. The control pulse (corresponding to the pump pulse) was first sent to the LSPCW for free-carrier generation, followed by the signal pulse (probe pulse) with a delay of Δt. The carrier density under the signal pulse at Δt was estimated from the loss of the signal output, which here depended on the FCA. Therefore, the temporal transition of the carrier density can be obtained by acquiring the signal's output power with changing Δt [21]. The output power is exponentially proportional to the FCA coefficient, which is itself proportional to the carrier density [22]. Therefore, we evaluated the signal loss by assessing the relative absorbance $-\log_{10}(P/P_0)$, where P and P_0 are the signal outputs with and without the control pulse, respectively. The optical setup for generating the control and signal pulses is detailed in Ref. [11]. After removing the control pulse by a bandpass filter, we measured the signal output by an optical power meter.

For maintaining the distance between the control and signal pulses in constant in the LSPCW, we set the control and signal pulses in the low-dispersion band. However, the control and signal wavelengths were separated for retaining only the signal pulse in the LSPCW output. The lengths of the control and signal pulses were set to 3.5 and 5.5 ps, respectively. By setting the input power of the signal pulse to 0.8 W, we suppressed the self-TPA of the signal and ensured a sufficient signal-to-noise ratio at the output. Figure 3(a) plots the signal absorbance versus Δt under various bias voltages V_{bias} and both low- and high-power control pulses ($P_{con} = 7.4$ and 30 W, respectively). When $\Delta t < 10$ ps, the signal pulse overlaps the control pulse and is excessively decreased by the TPA generated between them. Therefore, in the $\Delta t \geqslant 10$ ps region, the absorbance was originated by FCA alone. For a clear comparison, each absorbance was normalized by its value at $\Delta t = 10$ ps. The carriers were depleted by the reverse bias and the absorbance rapidly decreased at early Δt. The initial decline was accelerated at higher reverse biases. At later times, the decrease slowed under all bias voltages. This slow decrease might be sourced from FCA in the 200-μm-long SSC and the 30-μm-long Si wire waveguide. The initial rapid decline

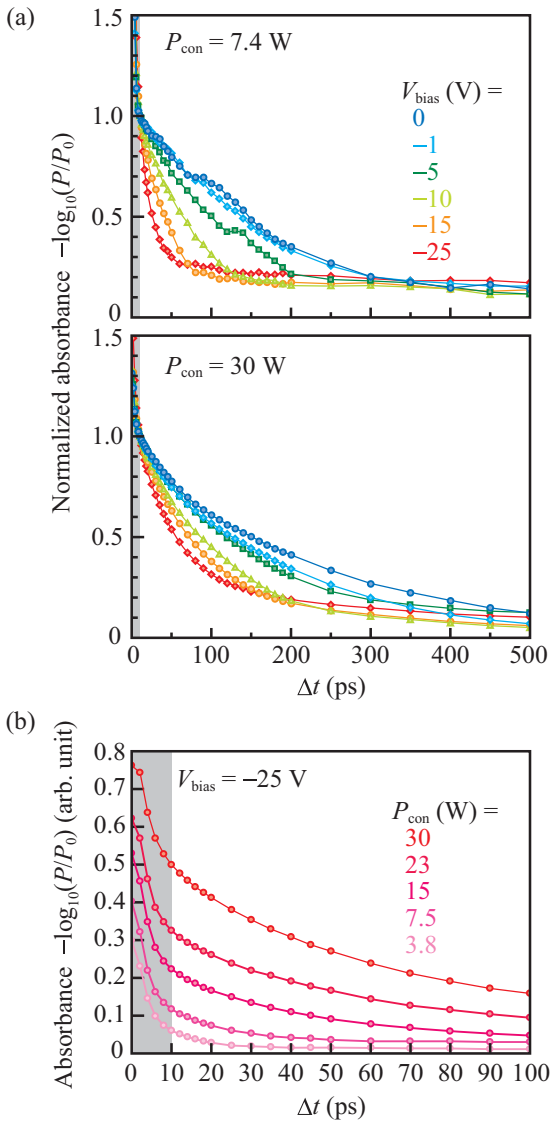

FIG. 3. Measured results of the carrier-depletion dynamics, evaluated by the absorbance at Δt for (a) different V_{bias} (distinguished by color) and P_{con} (distinguished by panels) and (b) different P_{con}. Gray region highlights the delay range in which the control and signal pulses overlap in the LSPCW.

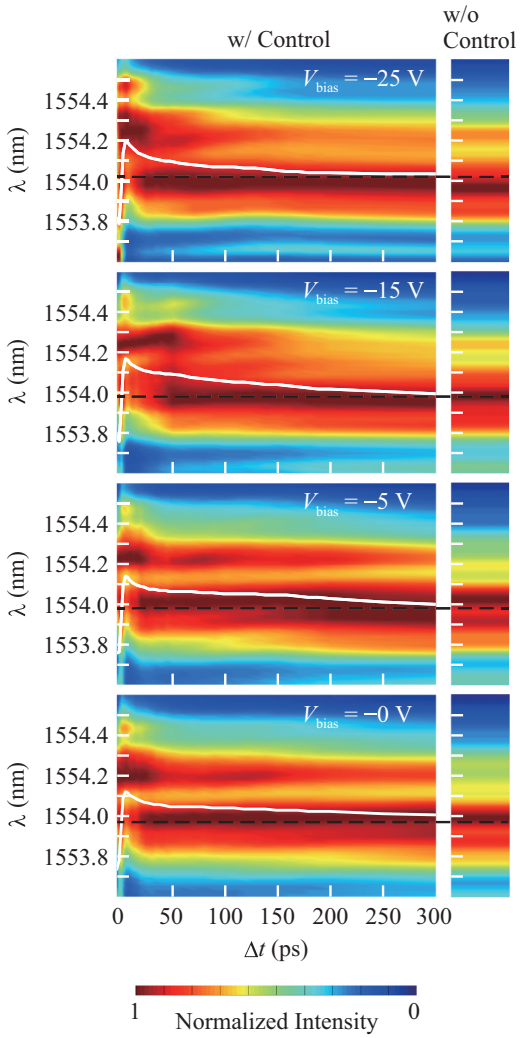

FIG. 4. Color maps of output signal spectra as a function of Δt, obtained at different V_{bias} values. The white solid and black dotted lines indicate the spectral centers of the output signals obtained with and without the control pulse, respectively.

in carrier numbers appeared to decelerate at higher powers of the control pulse, possibly reflecting a space-charge effect [23,24]. When excess carriers are generated, the free electrons and oppositely drifting holes create a space-charge field that internally cancels the depletion-layer field. Consequently, the depletion speed reduces. Comparing the absorbances on the same scale [Fig. 3(b)], increasing P_{con} still improved the depletion rate (i.e., the slope became large) when $\Delta t \geqslant 10$ ps. In the experiment, the carrier-depletion rate was raised at smaller Δt, higher V_{bias}, and higher P_{con}. Such a simple feature enables easy tuning of the redshift. The excess loss of the adiabatic-redshift tuning can also be estimated from these results. For $\Delta t = 10$ ps, $V_{bias} = -25$ V, and $P_{con} = 30$ W, the loss due to the tuning was approximately 5 dB.

IV. EXPERIMENT ON DYNAMIC REDSHIFT

The dynamic redshift was tested on the same setup as the above-mentioned pump-probe measurement. Here we observed the output spectrum of the signal pulse on an optical spectrum analyzer. The lengths and peak powers were set to 2.0 ps and 30 W, respectively, for the control pulse, and to 7.0 ps and 0.8 W, respectively, for the signal pulse. Figure 4 shows color maps of the signal output spectra as functions of Δt at different V_{bias} values. The signal spectra obtained with no control pulse are also exhibited for comparison. Regardless of V_{bias}, the signal pulse was redshifted when the control pulse was applied at $\Delta t \geqslant 10$ ps. Observing the spectral centers (white solid and black dotted lines), we confirm a larger redshift at higher voltage and smaller Δt. Moreover, the redshift diminished with increasing Δt. These trends confirm that the redshift originates in the dynamic carrier-depletion zone and increases with increasing speed of the depletion process. A feature arising from the carrier dynamics appeared also in the length of Δt yielding the redshift. As the reverse bias increased,

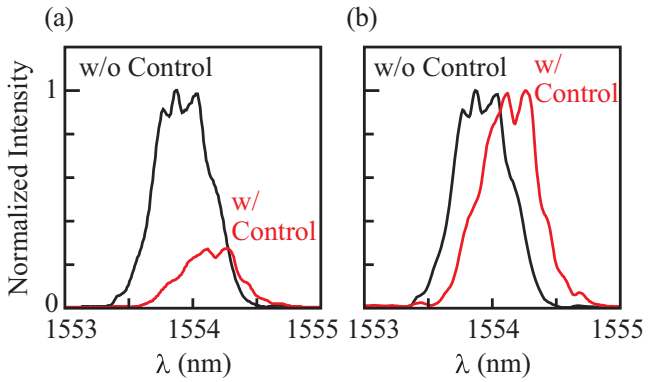

FIG. 5. Output signal spectra at the maximum redshift (0.21 nm), which are normalized by (a) the peak in the absence of the control pulse and (b) each peak.

the redshift was obtained in a comparatively short Δt span because the carrier depletion was completed within a short time. In contrast, at low reverse biases, the redshift was small and long lasting because the carriers were slowly depleted.

As Δt approached zero, the two pulses overlapped and the signal spectrum was expanded by the dynamic carrier generation and the optical Kerr effect of the control pulse. The spectral center of the signal then converted to blueshift. Here, the signal spectrum was expanded because the signal pulse was longer than the control pulse and was subjected (in part) to nonlinear effects [17]. However, a simple blueshift sourced from carrier generation can be achieved by applying a longer control pulse than the signal pulse [8]. Therefore, both the redshift and blueshift can be achieved merely by changing the input timing of the control pulse, thereby improving the flexibility of the adiabatic wavelength conversion.

For $\Delta t = 12$ ps, $V_{\text{bias}} = -25$ V, and $P_{\text{con}} = 30$ W, the redshift (evaluated in the spectral center) reached 0.21 nm (see Fig. 5). The ripple in these spectra was caused not by dynamic tuning, but by the transmission characteristics of the LSPCW. The redshift was clearly obtained, but was an order of magnitude smaller than the experimentally obtained adiabatic blueshift [2,4–8]. The redshift may have been diminished by slowdown of the carrier depletion under the space-charge effect [23,24]. The space-charge effect clearly appeared under a high-powered control pulse. Hence the improvement of the carrier-depletion rate increasing the control-pulse power and/or the n_g of the LSPCW (i.e., enhancing the slow-light effect) is restricted. However, the space-charge effect can be alleviated by optimizing the *p-i-n* junction structure. For example, it has been reported that the space-charge effect can be suppressed by optimizing the width of the intrinsic region and offset of the intrinsic-region center from the absorption region (corresponding to the LSPCW's center in this work) [24].

V. CONCLUSION

An adiabatic redshift was demonstrated in a *p-n*-diode–loaded Si LSPCW and a copropagating slow-light system. Carriers were generated by photon absorption and extracted in a reverse-biased *p-n* diode, enabling high-speed carrier depletion and effective redshift. We explored suitable conditions for the redshift using the pump-probe method, and confirmed that a large redshift can be simply induced by reducing the delay between the control and signal pulses, increasing the bias voltage, and boosting the control-pulse power. Redshifts of up to 0.21 nm were obtained in the experiments. At present, the redshift performance might be limited by the space-charge effect caused by excessive numbers of carriers, which degrades the carrier-depletion speed. We expect to resolve this problem by optimizing the structure of the *p-i-n* junction. To date, adiabatic wavelength conversion has enabled many advanced optical control techniques, as mentioned in the Introduction, but has utilized only the blueshift. The proposed redshift technique will improve and diversify the applications of wavelength conversion, leading to discoveries in physics and techniques such as pulse recovery and dynamic pulse acceleration and/or deceleration.

ACKNOWLEDGMENTS

This paper is based on results obtained from a project commissioned by the New Energy and Industrial Technology Development Organization (NEDO) and the Accelerated Innovation Research Initiative Turning Top Science and Ideas into High-Impact Values (ACCEL) Project of Japan Science and Technology Agency (No. JPMJAC1603).

[1] M. F. Yanik and S. Fan, Phys. Rev. Lett. **92**, 083901 (2004).
[2] S. F. Preble, Q. Xu, and M. Lipson, Nat. Photonics **1**, 293 (2007).
[3] T. Kampfrath, D. M. Beggs, T. P. White, A. Melloni, T. F. Krauss, and L. Kuipers, Phys. Rev. A **81**, 043837 (2010).
[4] J. Upham, Y. Tanaka, T. Asano, and S. Noda, Appl. Phys. Express **3**, 062001 (2010).
[5] M. C. Muñoz, A. Y. Petrov, and M. Eich, Appl. Phys. Lett. **101**, 141119 (2012).
[6] S. F. Preble, L. Cao, A. Elshaari, A. Aboketaf, and D. Adams, Appl. Phys. Lett. **101**, 171110 (2012).
[7] M. Castellanos Muñoz, A. Y. Petrov, L. O'Faolain, J. Li, T. F. Krauss, and M. Eich, Phys. Rev. Lett. **112**, 053904 (2014).
[8] K. Kondo and T. Baba, Phys. Rev. Lett. **112**, 223904 (2014).
[9] Y. Tanaka, J. Upham, T. Nagashima, T. Sugiya, T. Asano, and S. Noda, Nat. Mater. **6**, 862 (2007).
[10] D. M. Beggs, I. H. Rey, T. Kampfrath, N. Rotenberg, L. Kuipers, and T. F. Krauss, Phys. Rev. Lett. **108**, 213901 (2012).
[11] K. Kondo, M. Shinkawa, Y. Hamachi, Y. Saito, Y. Arita, and T. Baba, Phys. Rev. Lett. **110**, 053902 (2013).
[12] D. M. Beggs, T. F. Krauss, L. Kuipers, and T. Kampfrath, Phys. Rev. Lett. **108**, 033902 (2012).
[13] E. J. Reed, M. Soljačić, and J. D. Joannopoulos, Phys. Rev. Lett. **90**, 203904 (2003).
[14] E. A. Ulchenko, D. Jalas, A. Y. Petrov, M. C. Muñoz, S. Lang, and M. Eich, Opt. Express **22**, 13280 (2014).
[15] K. Kondo and T. Baba, Phys. Rev. A **93**, 011802 (2016).

[16] M. A. Gaafar, A. Y. Petrov, and M. Eich, ACS Photonics **4**, 2751 (2017).
[17] K. Kondo, N. Ishikura, T. Tamura, and T. Baba, Phys. Rev. A **91**, 023831 (2015).
[18] R. Konoike, H. Nakagawa, M. Nakadai, T. Asano, Y. Tanaka, and S. Noda, Sci. Adv. **2**, e1501690 (2016).
[19] M. Shinkawa, N. Ishikura, Y. Hama, K. Suzuki, and T. Baba, Opt. Express **19**, 22208 (2011).
[20] Y. Hinakura, Y. Terada, T. Tamura, and T. Baba, Photonics **3**, 17 (2016).
[21] A. C. Turner-Foster, M. A. Foster, J. S. Levy, C. B. Poitras, R. Salem, A. L. Gaeta, and M. Lipson, Opt. Express **18**, 3582 (2010).
[22] R. A. Soref and B. R. Bennett, IEEE J. Quantum Electron. **QE-23**, 123 (1987).
[23] K. J. Williams, R. D. Esman, and M. Dagenais, IEEE Photonics Technol. Lett. **6**, 639 (1994).
[24] K. J. Williams, R. D. Esman, R. B Wilson, and J. D. Kulick, IEEE Photonics Technol. Lett. **10**, 132 (1998).